International Journal of Heat and Fluid Flow 74 (2018) 198–208

Contents lists available at ScienceDirect

International Journal of Heat and Fluid Flow

journal homepage: www.elsevier.com/locate/ijhff

Qualitative and quantitative characterization of a synthetic jet mounted on a convex torpedo-like surface under cross-flow

Abhay Kumar, Ashish Karn*

Department of Mechanical Engineering, School of Engineering, University of Petroleum and Energy Studies, Energy Acres, Bidholi, Dehradun, Uttarakhand 248007, India

ARTICLE INFO

Keywords:
Synthetic jet
Vortex rings
Cross-flow
LDV
Flow visualization
Jet in cross flow

ABSTRACT

Understanding the fundamental flow physics of a synthetic jet in cross flow is important for a variety of engineering and scientific applications. In Particular, a synthetic jet mounted on a convex torpedo surface at high velocity ratios is of great importance for naval applications. However, despite exhaustive research done in this area, most of the studies have been conducted for synthetic jets on a flat surface and at low velocity ratios (ratio of average jet velocity and the cross-flow velocity). Studies at high velocity ratios particularly on a curved surface has largely not received much attention. Thus, the present study employs flow visualization and the laser doppler velocimetry (LDV) to qualitatively and quantitatively characterize such a synthetic jet under cross-flow conditions. Experiments have been conducted for quiescent flow conditions (i.e. 0 Hz) and at jet actuation frequencies of 1, 2, 4 and 6 Hz, at cross-flow velocities of 7.2, 20 and 32 cm/s. Our study indicates that the behaviour of synthetic jet changes significantly in the presence of cross-flow since it affects the formation, convection, and interaction among vortices, particularly at higher velocity ratios. Flow visualization provides interesting insights into the two major types of vortex rings and the interplay between the vortex structures and the boundary layer. Further, a comparison of the time-averaged velocity variation in the vertical direction reveals the formation of two local peaks at high velocity ratios and high actuation frequency of the jet. While the cross-flow is also found to be significantly affected by the high velocity ratio jet, the low velocity ratio jet in cross flow does not show substantial influence on the cross-flow except in regions close near the wall. The high velocity ratio jet shows the formation of a wake behind the jet region which is believed to be generated because of the blockage of the cross-flow created by the jet. Trailing jet and leading rings follow two different projectiles. Finally, a test-bed of LDV data has been reported in the study, which can prove useful in the validation of computational results of synthetic jets on a curved torpedo surface.

1. Introduction

Jets in a cross-flow (JICF) are of immense practical and engineering relevance for a variety of applications such as combustors (Ritchie et al., 2000), heat transfer enhancement (Chaudhari, et al., 2010), jet control (Smith and Glezer, 2002), propulsion & manoeuvring (Siekmann, 1962), drag reduction (Amitay, et al., 2001) and waste disposal into atmosphere or water bodies (Rodi, 1982). Many researchers have experimentally investigated the vortex dynamics and flow physics of a continuous jet as well as a synthetic jet in cross flow. Unlike a continuous jet, a synthetic jet can be defined as a series of vortex rings produced by repeated suction and expulsion of fluid through a small orifice, carrying no net mass flux and yet transferring linear momentum to the flow. Fig. 1 illustrates the process of a synthetic jet actuation. As shown in the figure, a synthetic jet actuation system is usually constituted of an oscillating diaphragm, a cavity opening and a fixed boundary that encloses to form a cavity. The oscillations of the diaphragm are created at one end of the cavity, while the other end consists of an orifice. The diaphragm oscillations regulate the fluid suction and ejection rates through the orifice.

Recently, a lot of research has been reported on the mean and turbulent flow quantities and mean flow characteristics of a synthetic jet. For instance, Sahni et al. (2010) have reported that a synthetic JICF yields three distinct types of effects on mean flow: (a) reduced velocity just upstream of the jet, (b) higher velocity downstream of the jet and (c) thickening of the boundary layer downstream of the jet. Wang et al. (2010) compared the jet velocity, flow flux, momentum flux and jet width at different duty cycles (suction period/blowing period) of a two-dimensional synthetic jet and found that the distributions of mean and turbulent quantities have similar features regardless of duty cycles.

* Corresponding author.
E-mail address: akarn@ddn.upes.ac.in (A. Karn).

https://doi.org/10.1016/j.ijheatfluidflow.2018.10.003
Received 26 June 2018; Received in revised form 24 October 2018; Accepted 24 October 2018

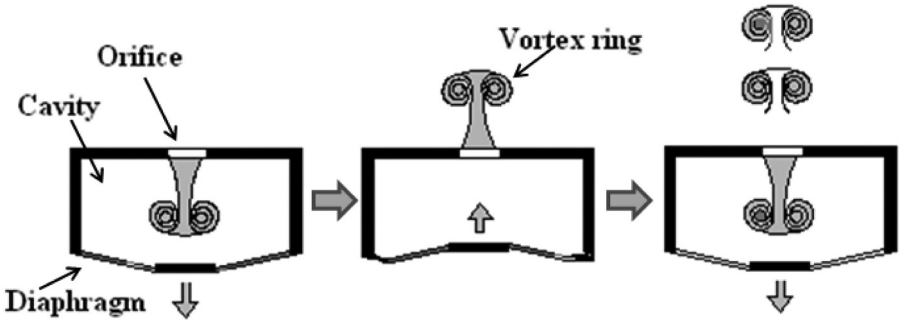

Fig. 1. Schematic of a synthetic jet actuation using orifice-diaphragm apparatus.

However, vortex pair generated at higher value of duty cycle convects faster exhibits stronger entrainment and higher momentum. The study of Gorden and Soria (2002) has established that 25–40% of the fluid volume drawn into the orifice cavity belongs to a narrow region that is 0.2 times the orifice diameter from the orifice periphery, and an extended region of 0.3 times the orifice diameter accounts for about 95% of the entire fluid volume sucked inside the orifice. Apart from these studies, there has also been a phenomenal amount of research reported exclusively on the vortex dynamics of jets in cross-flow. Prior research on both round continuous jet (Kelso, et al., 1996) and square continuous jet (Sau, et al., 2004) have illustrated the formation of horseshoe vortex, wall vortex and upright vortex along with counter rotating vortex pair for JICF. In comparison to the formation of a continuous or a synthetic jet in a quiescent flow, the flow physics of jets in cross flow is richer and more complex due to the stretching and tilting of vortex rings. Jabbal and Zhong (2008) observed three distinct types of vortical structures for synthetic JICF namely hairpin vortices, stretched vortex rings and tilted/distorted vortex rings when jet interacts with zero pressure gradient laminar boundary layer at low, intermediate and high velocity ratios, respectively. Other studies have also confirmed that the flow physics associated with synthetic JICF involves the formation of a train of discrete vortical structures, which locally promotes significant levels of mixing between the outer flow and flow near the wall helping the boundary layer to become re-energized (Prince, et al., 2012). Zhong et al. (2005) also focused on the interaction of a synthetic jet with wall boundary layer of a cross-flow at low Reynolds number. One cycle of synthetic jet forms two vortex rings, one during backward stroke where the vortex forms inside the cavity while the second one is generated outside the cavity during the forward stroke. The effect of Strouhal number, Reynolds number and velocity ratio on vortical structures of a synthetic jet is demonstrated. They found that the formation of vortex inside the cavity might contribute to a chaotic and turbulent fluid to be ejected in the subsequent cycle. Along similar lines, Duvigneau and Visonneau (2006) have explored the possible application of the synthetic jet-boundary layer interaction in enhancing the lift force of an airfoil by optimizing momentum coefficient, frequency and angle of synthetic jet with respect to the wall.

In the existing literature, there are a plethora of reports on the evolution of a vortex generated by a synthetic JICF. For a synthetic jet in a quiescent flow, the spacing between the vortex rings depends on the self-induced velocity of vortex ring and the rate of vortex generation i.e. actuation frequency. But, unlike a quiescent flow situation, in the presence of an external cross-flow, the vortex rings get convected in the direction of cross-flow after emerging from the orifice. Because of the nonlinear interaction between the cross-flow and vortex rings, the spacing between the vortex rings is strongly affected by the cross-flow conditions. Although the formation of these vortex rings in a cross-flow configuration may depend upon the fluid velocities in orthogonal directions, some studies have reported that the underlying flow physics is governed by the ratio of these fluid velocities (referred as velocity ratio, or $\tilde{v}$), over other physical parameters. For instance, Jabbal and Zhong (2010) concluded from their PIV measurements on a circular synthetic jet that at low velocity ratio ($\tilde{v} = 0.32$), the upstream side of vortex ring is found to be weaker than the downstream side leading to asymmetric development of vortex ring. Similar observation are also reported by Chaudhry and Zhong (2014), where the frequency is varied between 1 Hz to 6 Hz with an increment of 1 Hz and the velocity ratio is altered between 0.1 and 0.5 for each frequency. Crook and Wood (2001) using a circular synthetic JICF, actuating between 2 Hz to 10 Hz in water, concluded that the velocity ratio and vortex separation distance are key factors influencing the synthetic JICF. Milanovic and Zaman (2005) reported that the jet penetration height and its trajectory is solely a function of momentum flux ratio, which is equivalent to the velocity ratio (Jabbal and Zhong (2010)). A recent numerical study has ascribed the transition between the tilted vortex rings and the hairpin vortices to the velocity ratio in the range of 0.2–2 (Zhou and Zhong, 2010).

However, despite exhaustive research in the area of synthetic jets, almost all the prior research has focused on the synthetic jets in cross-flow on a flat surface or at low velocity ratios. There hardly exists any report that discusses the behaviour of a synthetic jet when it is mounted on a convex torpedo-like surface and particularly at high velocity ratios. A synthetic jet on a curved surface and at high velocity ratios is of immense interest for its possible usage in a torpedo or other similar naval applications. Further, it would be highly beneficial to carry out computational simulations of synthetic jets on a torpedo surface to characterize its efficacy at different flow conditions. Towards this end, experimental qualitative and quantitative data on characterization of a synthetic jet would be very much required for the validation of the simulations. Therefore, in this paper, we explore the flow behaviour of a circular synthetic jet flush mounted on the cylindrical torpedo-like surface in cross flow at different flow conditions through flow visualization and LDV. The present work not only presents interesting insights into the flow physics of synthetic jets on a curved torpedo surface at high velocity ratios, but may also serve as a test-bed of data for the validation of computational simulation results of other researchers. This paper is structured as follows: Section 2 provides the details for the experimental facility, and the setup. Subsequently in Section 3, we present results and discussion flow visualization and velocity measurements with a focus on the free water surface height and actuation frequency, followed by a final conclusion in Section 4.

2. Experimental setup and methodology

A torpedo shaped model with a built-in synthetic jet generation unit is fabricated, as shown in Fig. 2a, to study the behaviour of synthetic JICF environment. The diameter of the torpedo shaped model is 60 mm diameter and is stationed inside the horizontal and recirculating water tunnel with test section that has a square cross section with edge length of 400 mm. The diaphragm is made of nitrile coated nylon rubber sheet with 1.5 mm thick having inner and outer diameter equal to 33 mm and 43.5 mm respectively. A leaf spring made from 0.5 mm thick and 15 mm wide carbon steel strip is used to ensure a continuous contact

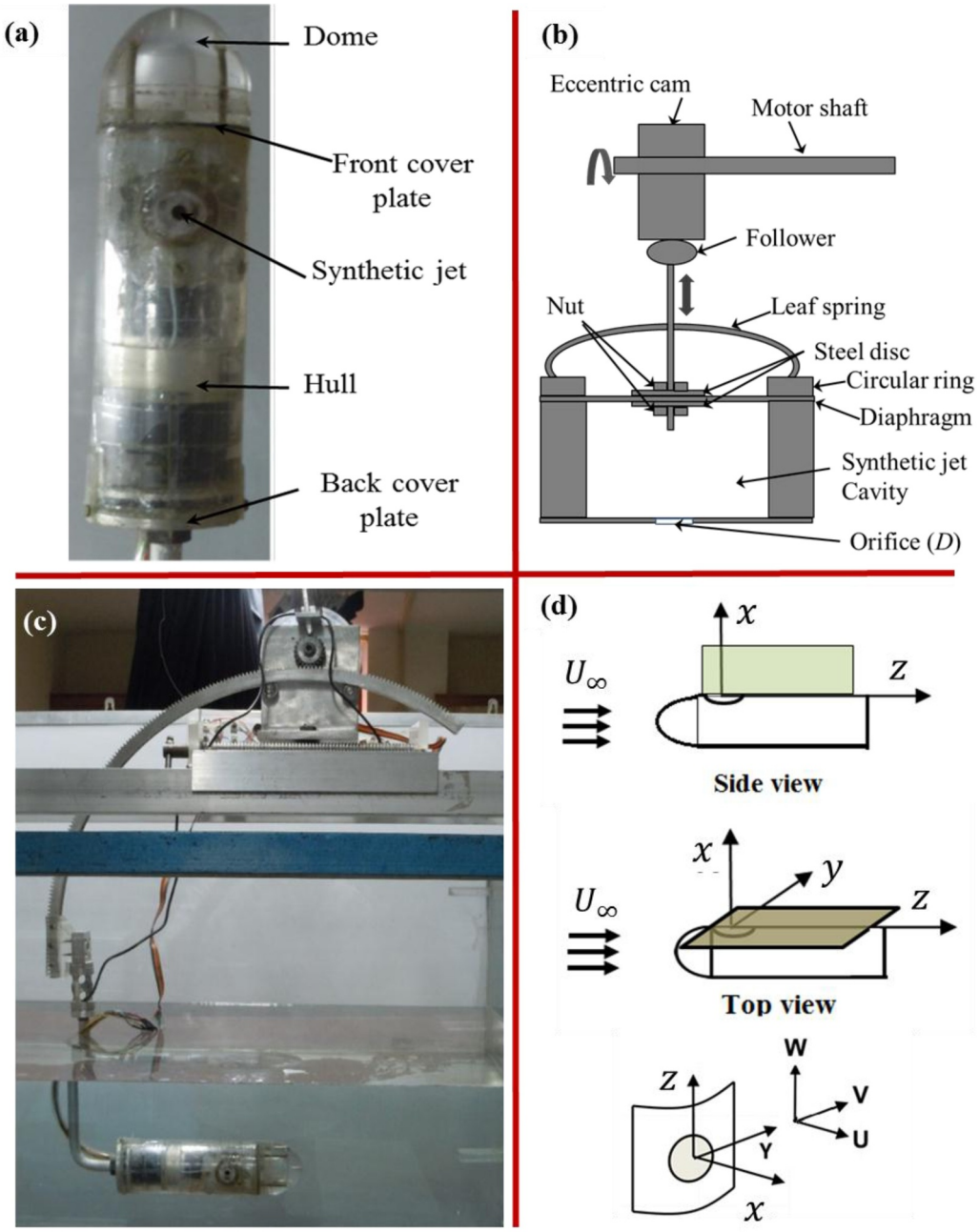

Fig. 2. (a) Experimental setup of the synthetic jet embedded in torpedo model, (b) details of actuation mechanism, (c) a picture showing torpedo model placed in the water tunnel for cross-flow experiments, and (d) schematic for axis notation and orifice orientation with imaging plane for torpedo shaped model.

Table 1
Values of cross-stream velocity and actuation frequency and the non-dimensional parameters at which experiments are conducted.

U_∞ (cm/s)	f_{act} (Hz)	Re_{SJ}	$\tilde{v}$
7.2	2	732	1.69
	4	1372	3.18
	6	2058	4.77
20.0	2	732	0.61
	4	1372	1.14
	6	2058	1.72
32.0	2	732	0.34
	4	1372	0.64
	6	2058	0.95

between the cam and the follower. The diameter (D) and the thickness of the circular orifice are both 6 mm. The cross-flow is obtained by putting the model inside the test section of a water tunnel as shown in Fig. 2b. The investigation is carried out in cross-flow for three different cross-flow velocities (7.2, 20.0 and 32.0 cm/s) for a fixed diaphragm displacement of 2 cm. Since, no flow is observed out of the orifice at an actuation frequency of 1 Hz, the measurements have been taken for frequencies of actuation equal to 2, 4, and 6 Hz. It should be noted that for simplicity, the actuation frequencies of 2.04 Hz, 3.92 Hz and 5.88 Hz have been rounded to its nearest integer and are expressed as 2 Hz, 4 Hz and 6 Hz, respectively. The bulk flow visualization is carried out using an incandescent light source. The fluorescein sodium is chosen as the dye for LIF imaging. The LIF images are captured with a resolution of 1280 × 1280 and a frame rate between 10 and 30 fps using Basler® A501-KC camera. Before the actuation of the diaphragm, the dye is

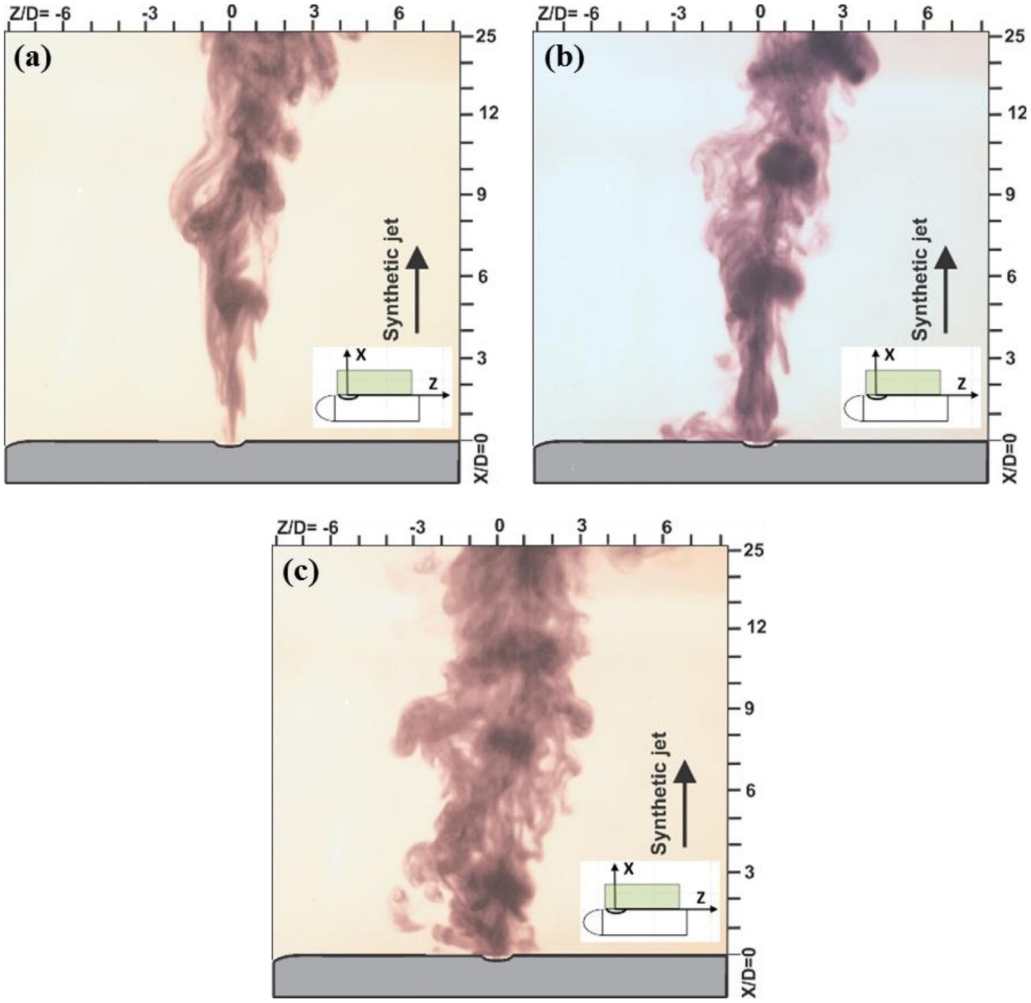

Fig. 3. Bulk flow visualization of the synthetic jet in side view for zero cross-flow velocity at (a) 2 Hz, (b) 4 Hz, and (c) 6 Hz.

slowly injected into the cavity of the synthetic jet through a precision syringe without disturbing the cross-flow in the water tunnel. Thereafter, the actuation of the diaphragm is started and the dye lasts for a few cycles, a duration typically sufficient to capture the flow phenomena.

Velocity measurements in streamwise (direction of synthetic jet ejection) and in cross-streamwise (cross-flow) direction are carried out using a five-beam LDV probe. These two projected views are shown in Fig. 2c as XZ-plane and XY-plane, respectively. Hollow glass spheres, coated with silver of diameter 8 μm −12 μm are used as external seeding particles. The laser source is a COHERENT® INNOVA-90, 4 W continuous wave Argon-Ion Laser. A plano-concave cylindrical lens of focal length (15 mm) is used to generating laser sheet of 1.5 mm thickness. The five-beam probe is stationed on a two-dimensional traverse that can move with a resolution of 6.25 μm, an accuracy of ± 300 μm and a repeatability of ± 10 μm in one direction. For the LDV measurements, the torpedo model is positioned 170 mm away from two transverse sidewalls, 120 mm from the bottom wall, and 120 mm from the free surface of the water in the test section.

The physical parameters involved in the present study are frequency (f_{act}) and amplitude of oscillation of the actuator (Δ), averaged jet exit velocity (U_{avg}), ejection time in a cycle (T_e), total cycle time (T), orifice diameter (D) and the geometrical parameters of the diaphragm such as inner cavity diameter (D_{ca}) and diameter of the disk (D_{cy}). The numerical values of D_{ca}, D_{cy} and D are 70 mm, 60 mm and 6 mm respectively. As suggested by Mohseni (2006), the ejected volume (V_d) for the diaphragm can be calculated as $V_d = \pi\Delta/8(D_{ca}^2 + D_{cy}^2)$. The average jet exit velocity and slug length (L) can be calculated as $U_{avg} = V_d/A_o T_e$ and $L = V_d/A_o$, where A_o denotes the cross-sectional area of the orifice. These physical parameters can be typically expressed in the terms of non-dimensional parameters such as Reynolds number, $Re_{SJ} = U_{avg} D/\nu$; Strouhal number, $St = f_{act} D/U_{avg}$ and Formation number, $Fn = L/D$, where ν and g represent the kinematic viscosity of water and acceleration due to gravity, respectively. It is also worth noting here that the formation number is merely a reciprocal of the Strouhal number. The velocity ratio ($\tilde{v}$) is the ratio of the slug velocity (U_{avg}) to the free or cross stream velocity (U_∞). The uncertainty in the actuation frequency of cam actuated synthetic jet is found to be ± 5%, whereas that in Reynolds and Strouhal number are equal to ± 5.2% and ± 0.5%, respectively. For an uneven sampling and a time duration of 60 s, a maximum fluctuation ± 3.7% around the mean is observed in the measured velocity components, whereas an uncertainty of ± 8% is obtained in the measurement of the velocity ratio. The blockage ratio based on cross sectional area is calculated to be 1.7%, which is within the acceptable range. Table 1 below presents the values of all the relevant parameters at which experiments are conducted in this study.

3. Results and discussion

3.1. Flow visualization

In this section, the bulk flow visualization using colour dye has been used to capture complex flow structures in the flow. Since it is customary to compare the jet flow under no cross-flow condition with the

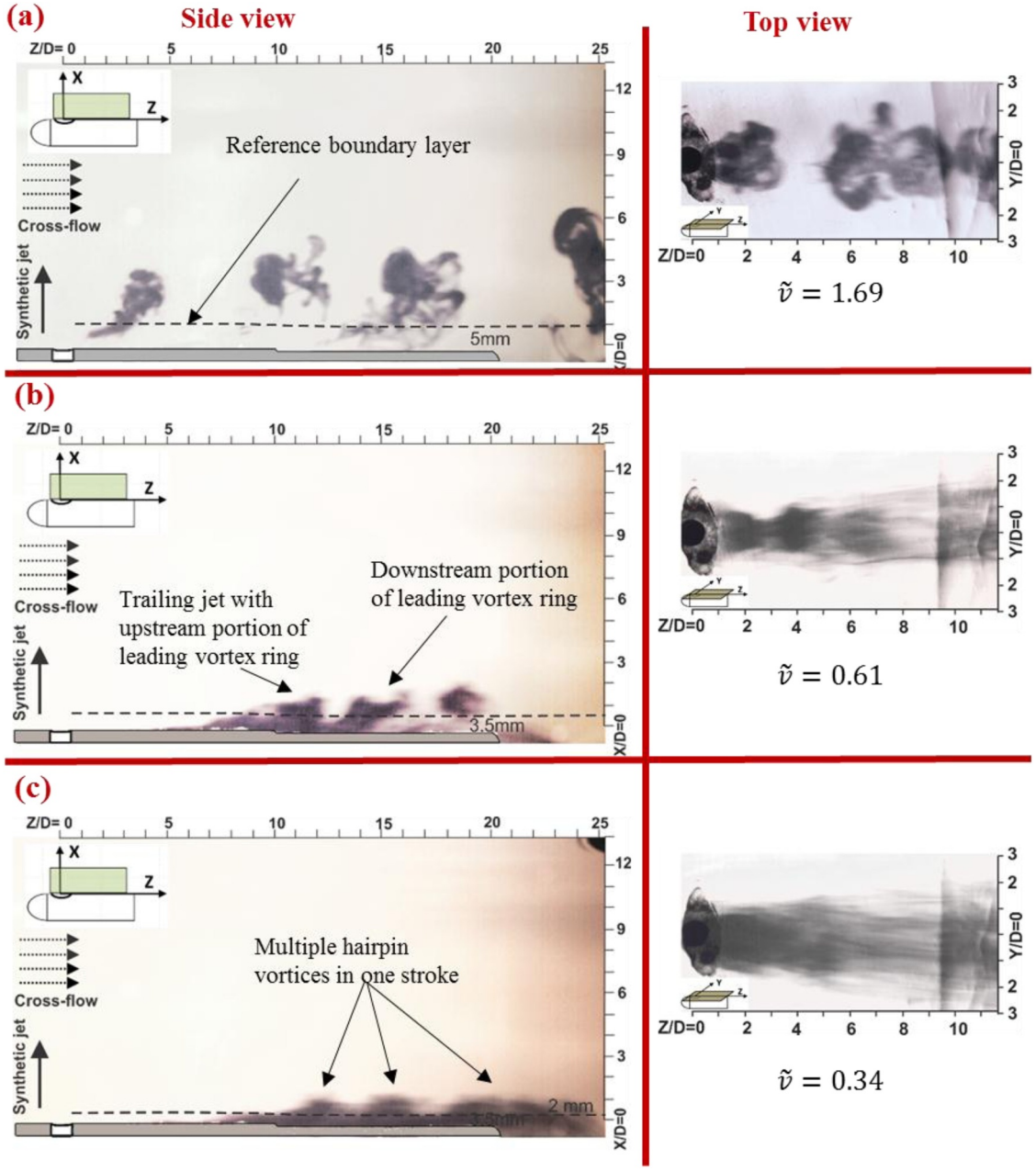

Fig. 4. Side and top visualization of the bulk flow of the synthetic jet at an actuation frequency of **2 Hz** and cross-flow velocity of (a) 7.2 cm/s, (b) 20.0 cm/s, and (c) 32.0 cm/s. The dashed line in side view is approximate boundary layer thickness with no synthetic jet. The observed flow structures are shown on the figure.

jet flow experiencing a cross-flow, the visualization of synthetic jet in quiescent flow has also been carried out. Fig. 3 presents the bulk flow visualization of a synthetic jet with zero cross-flow velocity for various actuation frequencies. The synthetic jet at 2 Hz as depicted in Fig. 3a, generates leading vortex with elongated weak trailing jet in comparison to the synthetic jet at 4 Hz shown in Fig. 3b, where the leading vortex ring is followed by strong coherent trailing jet. At an actuation frequency of 6 Hz (Fig. 3c), synthetic jet reveals a complex trailing jet showing greater spreading in transverse direction. The approximate value of the boundary layer thickness of the cross-flow without synthetic jet in place is measured from the estimate of transverse distance where local velocity becomes 0.99 U_∞. The boundary layer thickness so calculated is also termed as the reference boundary layer. The reference boundary layer thicknesses are 5, 3.5 and 2 mm for cross-flow velocities of 7.2, 20.0 and 32.0 cm/s, respectively. The relative positions of the boundary layer are also shown using dotted lines above the model surface wherever necessary. It should be pointed out here that the images of side view (XZ-plane) and top view (YZ-plane) are not in sync with each other and are taken at different instants of time.

The bulk flow visualization images of a synthetic jet at an actuation frequency of 2 Hz is shown in Fig. 4 at three different cross stream velocities (U_∞) equal to 7.2, 20.0 and 32.0 cm/s. In Fig. 4a, for U_∞ = 7.2 cm/s, the shear layer rolls to form vortex rings, which under the influence of cross-flow gets stretched in the stream-wise direction. The flow in the near field of the orifice experiences interactions between the vortex rings and the boundary layer causing an elongated leg between Z/D = 1 and 5. The distorted and stretched vortex ring crosses the reference boundary layer within an axial distance of Z/D = 5 and 10 and then travels in the direction of cross-flow without any significant movement in the upwards direction, which is orthogonal to the cross-flow direction. These types of structures generate strong fluid eruptions from the wall and result in the generation of new vortices in

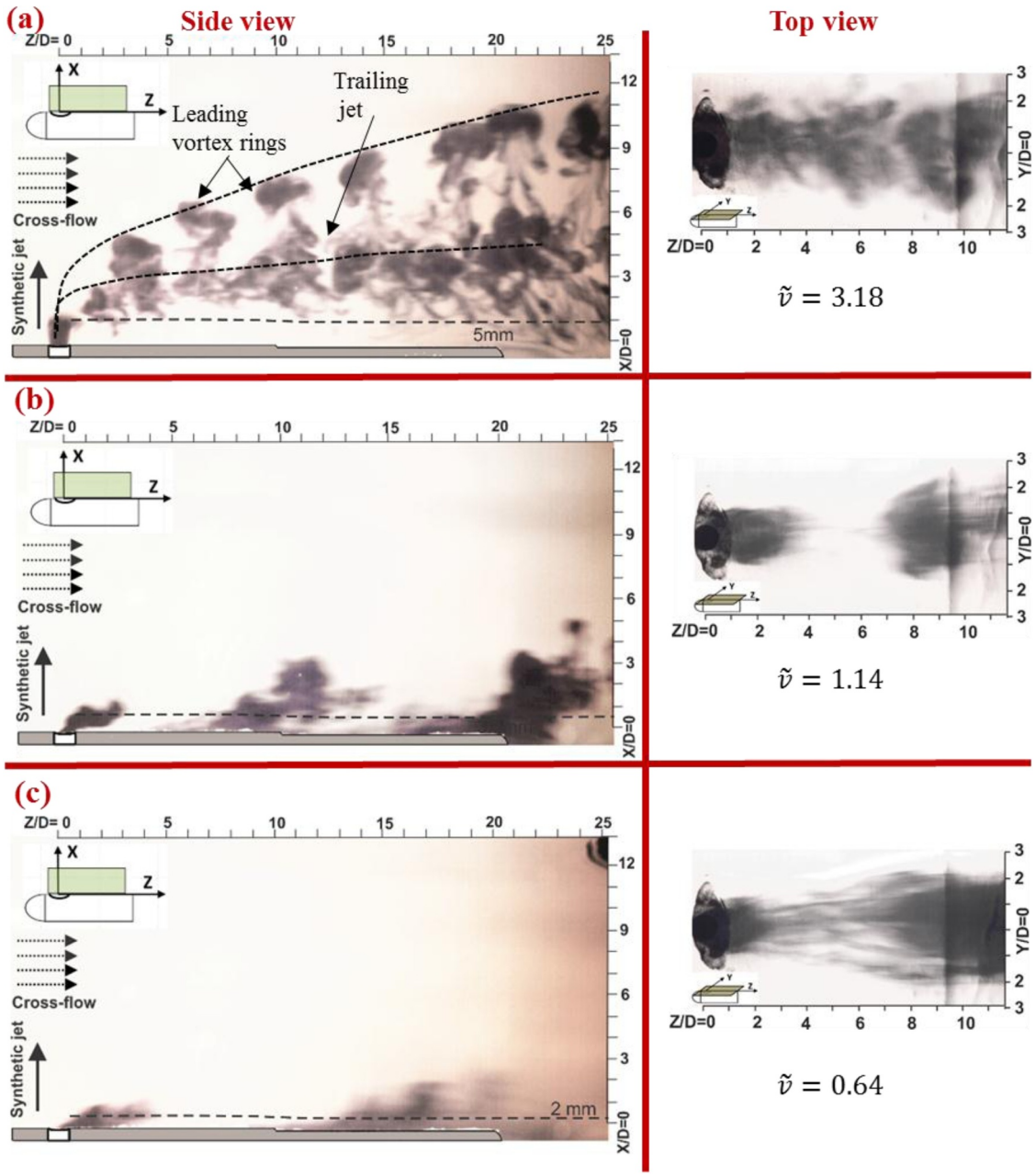

Fig. 5. Side and top visualization of the bulk flow of the synthetic jet at an actuation frequency of **4 Hz** and cross-flow velocity of (a) 7.2 cm/s, (b) 20.0 cm/s, and (c) 32.0 cm/s. The dashed line in side view is approximate boundary layer thickness with no synthetic jet. (a) shows the occurrence of tilted vortex rings, while (b) and (c) may have a combination of hairpin vortex rings or stretched vortex rings.

wake of the jet particularly at higher velocity ratios, and are known as induced stream-wise vortices (Chaudhry and Zhong, 2012). In both views of the visualization images, the two consecutive coherent structures are significantly far apart and consequently have a minimum interaction between them. The synthetic jet at same actuation frequency but at higher cross-flow velocity (U_∞ = 20.0 cm/s) depicted in Fig. 4b, experiences a higher stretching due to lower $\tilde{\nu}$ which reduces from 1.69 at U_∞ = 7.2 cm/s to 0.61 at U_∞ = 20.0 cm/s. Because of the higher cross-flow velocity, an asymmetric vortex ring is generated right at the outlet of the orifice. The downstream part of the vortex ring becomes quite stretched and travel downstream along the wall without experiencing any lift. The upstream portion of vortex ring pairs up with trailing jet of the preceding ring in the downstream and travels as a combined entity. When the cross-flow velocity is increased further to U_∞ = 32.0 cm/s, the $\tilde{\nu}$ decreases to 0.34. As a consequence, the synthetic jet becomes highly stretched and leads to interconnected and closely spaced hairpin vortices with large number of streamwise streaks (see corresponding top view) at a downstream location. At this $\tilde{\nu}$, the synthetic jet has transformed into a collection of highly stretched hairpin vortex rings, which remain close to the wall, with major portion of the rings residing within the reference boundary layer.

In a quiescent flow, the leading vortex rings are observed to be closely packed for an actuation frequency of 4 Hz with coherent trailing jet near the orifice (see Fig. 3b). However, in a cross-flow environment (U_∞ = 7.2 cm/s), the velocity and vorticity content of leading vortex ring is observed to be higher than the trailing jet. The difference in velocity between the leading vortex rings and the trailing jets leads to two different trajectories under the influence of cross-flow velocity as shown in Fig. 5a. The possible reason for the generation of such a flow structure lies in the significant disparity of $\tilde{\nu}$ experienced by leading and

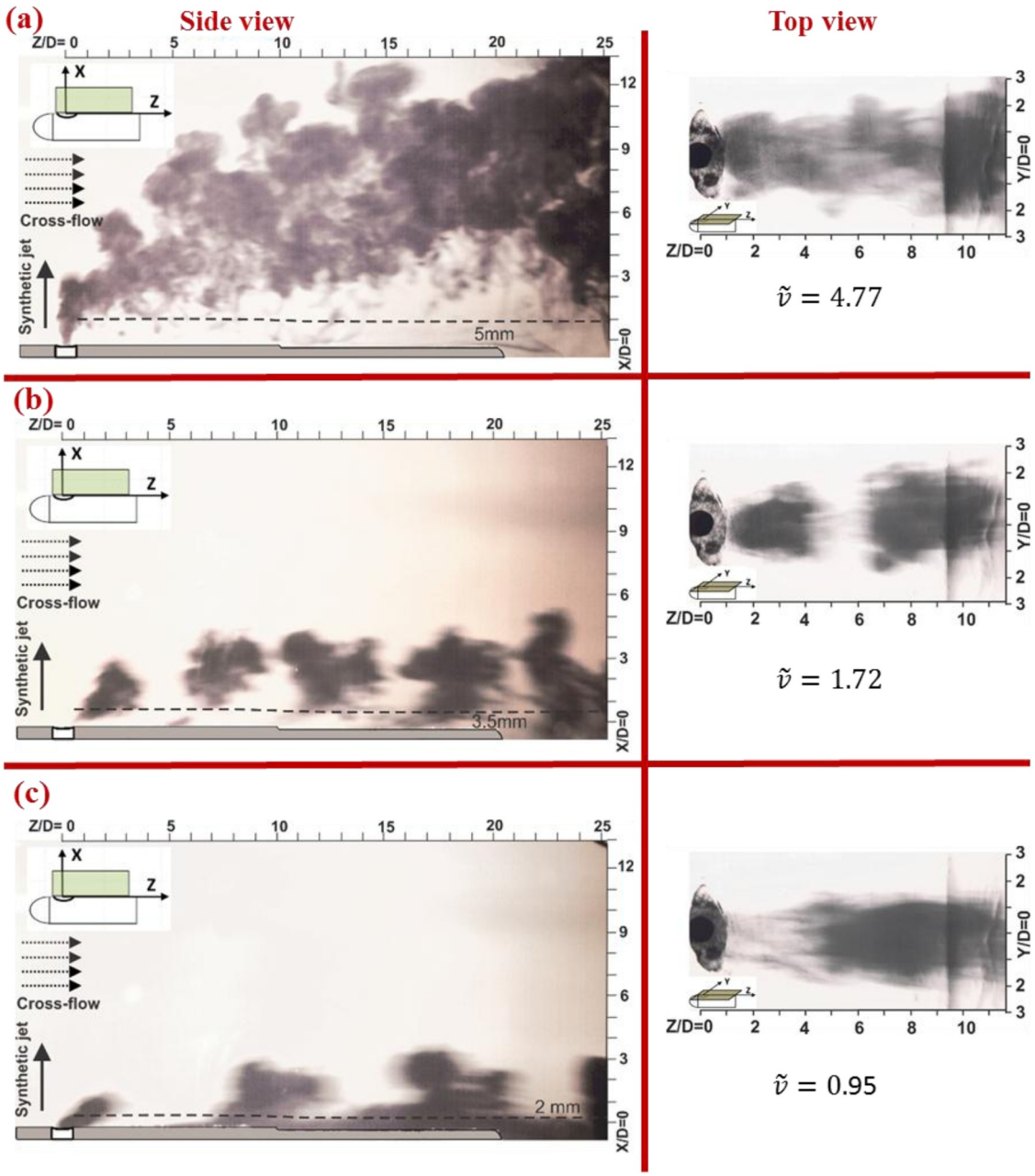

Fig. 6. Side and top visualization of the bulk flow of the synthetic jet at an actuation frequency of **6 Hz** and cross-flow velocity of (a) 7.2 cm/s, (b) 20.0 cm/s, and (c) 32.0 cm/s. The dashed line in side view is approximate boundary layer thickness with no synthetic jet. (a) and (b) show a combination of leading and tilted vortex rings, whereas (c) shows stretched vortex rings.

trailing jets due to their unequal self-induced velocities. The higher velocity of the leading vortex rings leads to the trajectory caused by the higher elevation angle at the orifice exit than that of trailing jet indicated by dotted lines. Unlike the synthetic jet in a quiescent flow condition, the leading vortex rings are well separated and distinguishable since the separation of the higher velocity leading vortex rings and the trailing jets does not allow the interaction between the two. On the other hand, the interaction of leading and trailing jets has been observed in the far field and results in the loss of the coherency of the jet structures. The trailing jets are also found to be interlinked because of their low convection velocity and interact with each other in downstream (Fig. 5a). The entire jet travels in the cross-flow direction but remains above the reference boundary layer. An increase in cross-flow velocity to U_∞ = 20.0 cm/s, the trailing jets become weaker as large amount of fluid gets accumulated in the leading region of the vortex, lifting the vortex structures upwards. However, they remain partially within the reference boundary layer (side view in Fig. 5b). These stretched vortex ring structures are the intermediate forms of hairpin and tilted vortex rings. The stretched vortex rings differ from hairpin vortex rings in the sense that maximum amount of ejected fluid having higher vorticity is accumulated in the head region of the vortex rather than in counter rotating vortex legs (Chaudhry and Zhong (2014)). The flow structures developed at an actuation frequency of 4 Hz and cross-flow velocity of 32.0 cm/s depicted in Fig. 5c is almost similar to the flow structures shown in Fig. 4c where the actuation frequency and cross-flow velocity is 2 Hz and 32.0 cm/s respectively. The number of vortex rings within equal axial length of the flow domain at 4 Hz actuation frequency is more than that at 2 Hz for equal cross-flow velocity, thus indicating a lower interaction of two consecutive vortex rings for 2 Hz. The bulk flow visualization images taken for actuation

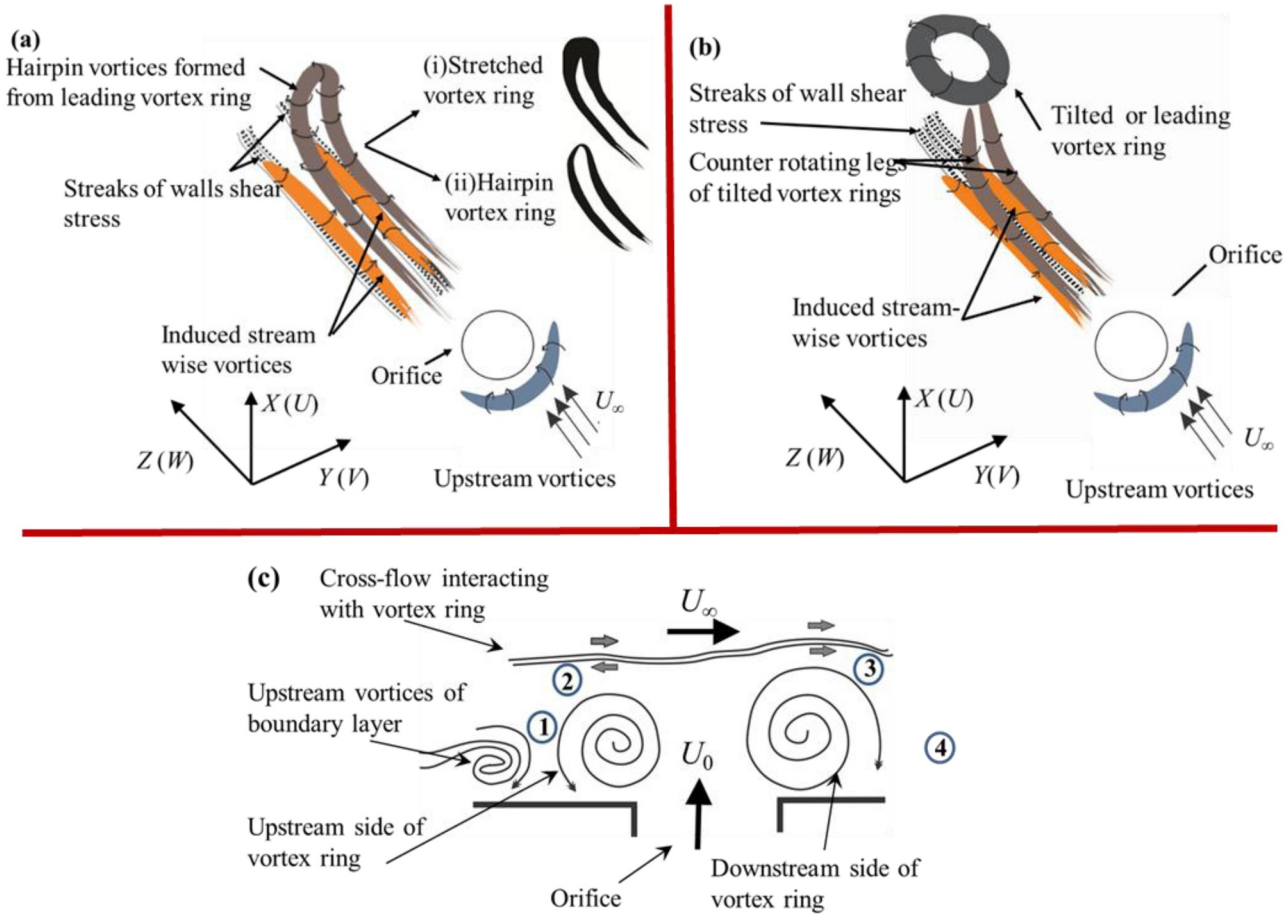

Fig. 7. Schematic representing the synthetic JICF having (a) hairpin and stretched vortices and (b) tilted and distorted vortex ring with stretched trailing jet (c) evolution of synthetic JICF.

frequency of 6 Hz are shown in Fig. 6 at three cross-flow velocities. For a cross-flow velocity of 7.2 cm/s, the elevation angle and penetration depth at 6 Hz is much higher in comparison to those at 4 Hz as shown in Fig. 6a. The other significant difference between two flow structures at two frequencies is that the leading vortex rings and trailing jet interacts due to lower difference in their ejection velocity giving a sparsely distributed flow structures.

The flow trajectories and evolution of vortex rings at 6 Hz in Fig. 6b for a velocity of 20.0 cm/s and Fig. 6c for a velocity of 32.0 cm/s closely resemble with those shown in Fig. 4a at 2 Hz (and velocity of 7.2 cm/s) and Fig. 5b at 4 Hz (and velocity of 20.0 cm/s), respectively. The probable reason for this behaviour is due to close match of velocity ratios between the two different cases having different actuation frequencies. Analysis of the flow structures of visualization images at different frequencies and cross-flow velocities reveals that the flow structures and evolution of synthetic JICF primarily depend on resulting $\bar{v}$ which in turn depends on both the actuation frequency and cross-flow velocity. For a given $\bar{v}$, Milanovic and Zaman (2005) found that the penetration depth collapses to a single point when scaled with the ratio of square of cross-flow velocity to square of synthetic jet velocity.

Based on the analysis of the flow images and the reported research available in the literature (Chaudhary and Zhong, 2014, Jabbal and Zhong (2008)), it can be concluded that the vortices or vortex rings in synthetic jet can be classified into two major groups: (a) stretched vortex ring and (b) tilted and distorted vortex ring. Vortex rings, which occur at low $\bar{v}$ and remain attached to wall result in the formation of either a hairpin vortex ring or a stretched vortex ring, the basic difference between the two lying in the location of maximum vorticity as shown in Fig. 7. If the legs of hairpin structures contain maximum amount of vorticity, they are known as *hairpin vortices*. However, if the maximum amount of vorticity is concentrated at the upward-lifted head region and gets stretched by the cross-flow because of being partially above the boundary layer, it is called a *stretched vortex* ring. In the case of a *tilted vortex ring*, the leading vortex ring detaches itself from the wall and penetrates into the core cross-flow due to higher momentum and induced velocity. If the trailing jet gets stretched in the form of hairpin structure behind the tilted vortex ring, then it is seen to shed itself as coherent structures. The counter rotating legs of stretched hairpin vortices in Fig. 7a or the counter rotating stretched trailing jet in Fig. 7b are expected to induce two cross-streamwise vortices beneath them because of the presence of wall. The interaction between the vortices of counter rotating legs with induced cross-streamwise vortices draws higher momentum fluid near the wall from core cross-flow and redistributes the vorticity content of the boundary layer. Since at low $\bar{v}$ the maximum portion of the length of hairpin legs are close to the wall, they create a downwash bringing high momentum fluid from core flow towards the wall and thus increase the local shear stress.

Further, it is also expected that because of the downwash, two streaks of walls shear stress are formed beneath the induced cross-streamwise vortices as shown in Fig. 7. The other vortices are also formed on the upstream side of the orifice and are termed as upstream vortices or horse-shoe vortices (Wen and Tang, 2012). The magnitude and time-scale of the upstream vortices are expected to depend on both $\bar{v}$ and the ejection period of synthetic jet. The correlation between the observed flow structures in our experiments vis-à-vis the flow physics discussed above is clearly evident from Figs. 4–6.

The tilting or stretching of synthetic JICF is a key feature in the formation of hairpin vortices aligned with the cross-flow direction.

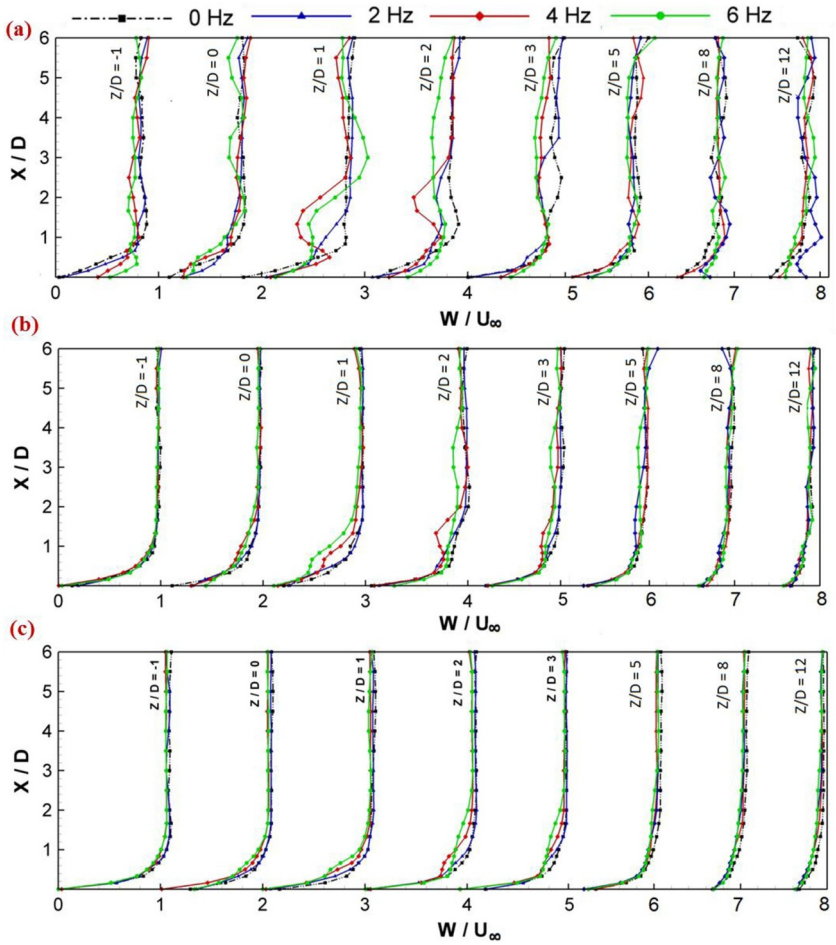

Fig. 8. Time-averaged stream-wise velocity component (W) at eight different downstream locations at an actuation frequency of 0, 2, 4 and 6 Hz and at a cross-flow velocity of (a) U_∞ = 7.2 cm/s, (b) 20.0 cm/s and (c) 32.0 cm/s. The curves at different frequencies are shifted by a step-size of unity on the x-axis for enhancing clarity.

Within the boundary layer, the vortex tilting or stretching occurs because of the vorticity variations of vortex ring at orifice exit. The sectional view of the vortex rings gives two counter-rotating (CR) vortices separated by a distance equal to the diameter of the ring. Due to the cross-flow, the vorticity strength of upstream counter-rotating vortices of synthetic jet is adversely affected by both (i) the upstream vortices also called horse-shoe vortices generated due to blockage of the incoming cross-flow boundary layer by the jet and (ii) the shear layer of incoming flow. The regions which affect the upstream CR vortices are indicated as '1' and '2' in Fig. 7c. In region '1', the rotation of CR vortices is opposite to that of the horse-shoe vortices while in region '2', the top part of CR vortex is opposed by cross-flow velocity as shown in Fig. 7a. On other hand, the downstream CR vortices is favoured by cross-flow at the top (region 3) because both have identical sense of flow motion. Especially at higher $\bar{v}$, the blockage of cross-flow by the jet creates a wake region (region 4) in the downstream side of synthetic jet and may lead to enhancement of the strength of downstream CR vortices. When the suction stroke begins, the large amount of fluid is sucked inside the cavity from upstream side because of the lower velocity of the cross-flow caused by the blockage of the jet in this region. From the above discussion, it is quite evident that the combined effect of shear layer interaction in the four regions indicated earlier produces an asymmetric vortex ring with varying vorticity content around the circumference of the ring. The upstream part of the ring has minimum vorticity while the vorticity content increases slowly towards the downstream along the circumference. Consequently, this asymmetric distribution of vorticity results in a doughnut shape ring having non-uniform cross-sectional area, being minimum at upstream while maximum at downstream. Since the variation in vorticity causes a variation in self-induced velocity, the differential lift is experienced by the vortex ring. The downstream side of vortex ring experiences higher lift in comparison to the upstream side. In case of the hairpin vortices, the difference of self-induced velocity is such that the downstream part of leading vortex ring lifts up while the upstream part remains attached to the wall and interact with the boundary layer. The velocity variation within the boundary layer further provides a differential shearing force on the asymmetric vortex ring causing a huge stretching in cross-stream direction forming the legs of hairpin vortices.

3.2. Time averaged velocity field

The flow visualization results mainly provide the instantaneous flow field of a synthetic JICF. The time-averaged field provides the large scale coherent structures which are generally boundary dependent. The cross-flow component of velocity (V) and the vertical velocity component along jet axis (U) are averaged over 60 cycles of synthetic jet actuation. The time-averaged flow field in the XZ-plane (side view) for torpedo shaped model placed inside the test section of water tunnel has been measured using LDV. A fine grid is used in the XZ-plane for the velocity measurements close to the wall, the nearest point to the wall being 0.25 mm, varying by the same amount till a distance of 6 mm. Above this region, a coarse grid is used and the measurements are taken at an interval of 0.5 mm. In our experiments, the minimum boundary layer thickness is approximately 2 mm, and our measurement strategy

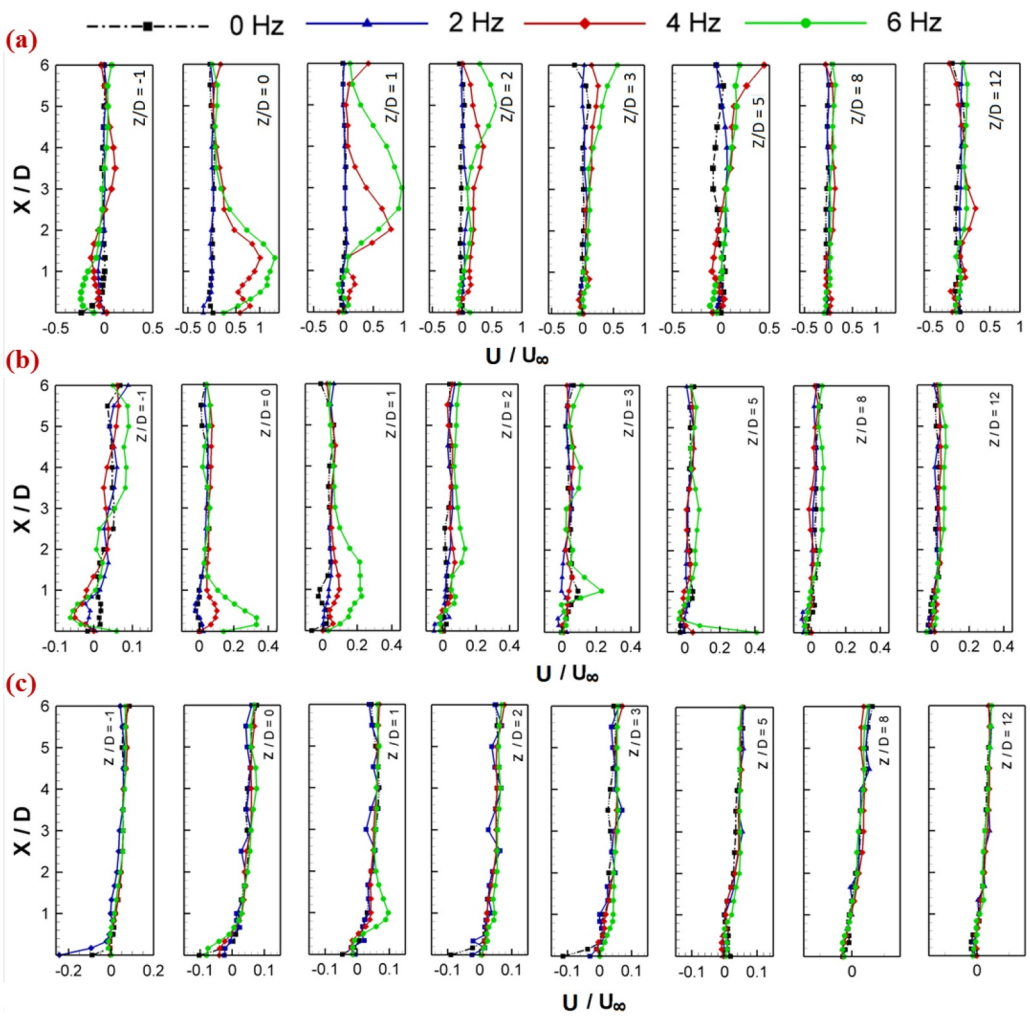

Fig. 9. Time-averaged vertical velocity component (U) at eight different downstream locations at an actuation frequency of 0, 2, 4 and 6 Hz and at a cross-flow velocity of (a) $U_\infty = 7.2$ cm/s, (b) 20.0 cm/s and (c) 32.0 cm/s. The curves at different frequencies are shifted slightly on the x-axis for enhancing clarity.

ensures that there are at least 7–8 points at every Z location. The measurements are taken for all three values of cross-flow velocities. The vertical variation of velocity components at eight distinct locations ($Z/D = -1$, 0, 1, 3, 5, 8 and 12) on XZ plane passing through the centre of the orifice is shown in Fig. 8. The actuation frequency has been varied in the range of 0–6 Hz (0, 2, 4 and 6 Hz) for three different cross-flow velocities ($U_\infty = 7.2$, 20.0 and 32.0 cm/s). The velocity variation with no jet indicated using solid symbols and dashed line is taken as reference for comparing the velocity variation for the various frequencies.

For a cross-flow velocity of $U_\infty = 7.2$ cm/s, the vertical variations of cross-flow velocity component for various frequencies at different axial locations are depicted in Fig. 8. The velocity variations at an upstream location of the orifice, $Z/D = -1$ reveal almost a similar distribution near the wall except for frequencies of 4 and 6 Hz where a region with positive velocity has been observed. The distribution of vertical velocity reveals the evidence of the negative velocity regions shown in Fig. 8a at the same location. As discussed earlier, the synthetic jet draws greater amount of fluid from the upstream portion of orifice at higher frequencies thus increasing the cross-flow velocity within the boundary layer along with a downward vertical velocity (negative velocity). The cross-stream velocity component (W) decreases near the orifice exit ($Z/D = 0$) due to combined effect of blockage of cross-flow during ejection stoke and suction of boundary layer fluid during suction stroke. At locations downstream of the orifice, the cross-flow velocity near the wall is found to show velocity deficit in comparison to the reference velocity variation and two localized peaks indicating the two trajectories of vortices namely leading and trailing ones (see Figs. 5a and 6a). With increasing downstream distance, the deficit decreases indicating weakening of the vortices in the two rows possibly because of the vortex diffusion and entrainment of outer fluid into the jet region. The variation of vertical velocity component (U) (Fig. 9a) at locations downstream of orifice shows positive velocity for the two higher frequencies (4 and 6 Hz) indicating the upward motion of the jet, the magnitude of which decreases with increasing downstream distance. Also increasing width of the velocity surplus in vertical velocity component indicates the spreading nature of the jet with increasing axial distance. The reason for this behaviour may be explained as follows: The train of vortices generated in synthetic jet produces a shielding effect to the cross-flow. This shielding generates a low-pressure region behind the synthetic jet in downstream and results in reduction of the velocity. This wake region draws more fluid from the adjoining region, thereby increases the spreading. From the velocity variation, the blockage effect on cross-stream velocity is found to be limited to $Z/D = 5$ beyond which no substantial velocity deficit is observed. Similar observation has also been reported by Lardeau and Leschziner (2011) in their numerical study of a circular synthetic JICF.

At higher cross-flow velocities ($U_\infty = 20.0$ and 32.0 cm/s), the vertical variation of the two components of velocity does not reveal significant variation, in comparison to the baseline case. It is obvious that the higher cross-flow velocity corresponds to a lower velocity ratio. This in turn diminishes the relative strength of the jet experiencing an increasing higher cross-flow velocity. Fig. 8b confirms this through a

small velocity deficit near the wall at locations close to the orifice. Similar observation has also been observed in the case of vertical velocity shown in Fig. 9b, where changes have been observed only at the highest frequency. The velocity variations for $U_\infty = 32.0$ cm/s at various frequencies (see Fig. 8c and Fig. 9c) reveal even lower influence of the jet on the cross-flow velocity except close to the wall. This is clearly expected at higher cross-flow velocity, the jet structures confine themselves near the wall unlike at higher velocity ratio where the cross-flow gets affected significantly over the entire vertical span of the flow domain.

4. Conclusions

The current study focuses on the qualitative and quantitative characterization of a synthetic jet mounted on a curved torpedo surface at different flow conditions and at different points in the flow field through flow visualization and LDV measurements, respectively. In the presence of a cross-flow, the behaviour of synthetic jet changes significantly particularly at higher velocity ratio as the formation, convection, and interaction among vortices are influenced by the cross-flow. Analysis of the flow visualization images reveal two major types of vortex rings: (a) stretched vortex ring and (b) tilted and distorted vortex ring. The tilting or stretching of synthetic JICF is a key feature in the formation of hairpin vortices aligned with cross-flow when residing within the boundary layer. Comparison of time-averaged velocity variation in the vertical direction reveals the formation of two local peaks at higher velocity ratio and higher frequency of actuations. The high velocity ratio jets are found to significantly alter the cross-flow. On the other hand, the low velocity ratio JICF does not show substantial influence on the cross-flow except near the wall. The high velocity ratio jet shows the formation of wake behind the jet region which is believed to be generated because of the blockage of the cross-flow created by the jet and it was observed that the trailing jet and leading rings follow two different paths. Finally, it was also found that velocity ratio is one single parameter that characterizes the flow physics of a synthetic jet in cross-flow, over other parameters like frequency of actuation and cross-flow velocity.

Acknowledgements

The first author gratefully acknowledges the contribution of Dr. P. K. Panigrahi and Dr. A. K. Saha for their support and guidance in carrying out the experiments at IIT Kanpur.

Supplementary materials

Supplementary material associated with this article can be found, in the online version, at doi:10.1016/j.ijheatfluidflow.2018.10.003.

References

Amitay, M., et al., 2001. Modification of the Aerodynamics Characteristics of an Unconventional Airfoil Using Synthetic Jet Actuators. AIAA Journal 39 (3), 361–370.
Chaudhari, M., Puranik, B., Agrawal, A., 2010. Effect of orifice shape in synthetic jet based impingement cooling. Experimental Thermal and Fluid Science 34, 246–256.
Chaudhry, I., Zhong, S., 2012. Understanding the interaction of synthetic jet with the flat plate boundary layer. In: International Conference on Advanced Research in Mechanical Engineering. Trivendum.
Chaudhry, I., Zhong, S., 2014. A single circular synthetic jet issued into turbulent boundary layer. Journal of Visulisation 17 (2), 101–111.
Crook, A., Wood, N., 2001. Measurement and visualisations of synthetic jets. s.n., Nevada.
Duvigneau, R., Visonneau, M., 2006. Optimization of a synthetic jet actuator for aerodynamic stall control. Computers and Fluids 35, 624–638.
Gorden, M., Soria, J., 2002. PIV measurements of a zero-net-mass-flux jet in cross flow. Experiments in Fluids 33, 863–872.
Jabbal, M., Zhong, S., 2008. The near wall effect of synthetic jets in a boundary layer. International Journal of Heat and Fluid Flow 29, 119–130.
Jabbal, M., Zhong, S., 2010. Particle image velocimetry measurements of the interaction of synthetic jets with a zero-pressure gradient laminar boundary layer. Physics of Fluids 22, 1–17.
Kelso, R., Lim, T., Perry, 1996. An experimental study of round jets in cross-flow. J. Fluid Mech 306, 1111–1144.
Lardeau, S., Leschziner, M.A., 2011. The interaction of round synthetic jets with a turbulent boundary layer separating from a rounded ramp. J. Fluid Mech. 638, 172–211.
Milanovic, I., Zaman, K., 2005. Synthetic jet in cross flow. AIAA 43 (5), 929–940.
Mohseni, K., 2006. Pulsatile vortex generators for low-speed maneuvering of small underwater vehicles. Ocean Engineering 33, 2209–2223.
Prince, S., Khodagolian, V., Gaind, R., 2012. An experimental study of a pulsed air jet and an acoustic jet on a low speed turbulent boundary layer. In: 28 th International congress of the Aeronautical sciences. Brisbane, AU.
Ritchie, B.D., Majumdar, D., Seitzman, J., 2000. Mixing in Coaxial jets Using Synthetic jet Actuators. AIAA 0404.
Rodi, W., 1982. Turbulent buoyant jets and plumes. s.n., Pergamon.
Sahni, O., Wood, J., Jansen, K., Amitay, M., 2010. 3-D Interactions between a Finite-Span Synthetic Jet and a Cross-Flow. In Press, Journal of Fluid Mechanics.
Sau, A., Sheu, T., Hwang, R., Yang, W., 2004. Threee dimensional simulation of square jets in cross-flow. Physical Review E 69.
Siekmann, J., 1962. On a pulsating Jet from the end of a tube, with application to the propulsion of certain aquatic animals. Journal of Fluid Mechanics 15 (3), 399–418.
Smith, B.L., Glezer, A., 2002. Jet vectoring using synthetic jets. J. Fluid Mech. 458, 1–34.
Wang, J., Shan, R., Zhang, C., Feng, L., 2010. Experimental investigation of a novel two-dimensional synthetic jet. European Journal of Mechanics B/Fluids 29, 342–350.
Wen, X., Tang, W., 2012. Interaction of synthetic jets with laminar and turbulent boundary layers. s.n., Launceston.
Zhong, S., Millet, F., Wood, N., 2005. The behaviour of circular synthetic jets in a laminar boundary layer. The Aeronautical Journal 461–470.
Zhou, J., Zhong, S., 2010. Coherent structures produced by the interaction between synthetic jets and a laminar boundary layer and their surface shear stress patterns. Computers and Fluids 39, 1296–1313.